BULLETIN DE L'ASSOCIATION MINERALOGIQUE DU CANADA

THE CANADIAN MINERALOGIST

JOURNAL OF THE MINERALOGICAL ASSOCIATION OF CANADA

Volume 33 December 1995 Part 6

The Canadian Mineralogist
Vol. 33, pp. 1157-1166 (1995)

ELECTRON-LOSS NEAR-EDGE STRUCTURE (ELNES) AS A PROBE OF VALENCE AND COORDINATION NUMBER

LAURENCE A.J. GARVIE

Department of Geology, Arizona State University, Tempe, Arizona 85287-1404, U.S.A.

PETER R. BUSECK

Departments of Geology and Chemistry, Arizona State University, Tempe, Arizona 85287-1404, U.S.A.

ALAN J. CRAVEN

Department of Physics and Astronomy, University of Glasgow, Glasgow G12 8QQ, U.K.

Abstract

We used parallel electron energy-loss spectroscopy (PEELS) in a scanning transmission electron microscope (STEM) equipped with a cold field-emission gun to acquire high-resolution spectra. Detailed analysis of electron-loss near-edge structure (ELNES) of core-loss edges provides chemical information about the oxidation state and site symmetry of the excited atoms. In many cases, the ELNES exhibits a shape that is dependent upon the nearest-neighbor coordination and represents a "fingerprint" of this coordination. Gaudefroyite, $Ca_4Mn_3(BO_3)_3(CO_3)(O,OH)_3$, contains several light elements and, as such, is ideal for a demonstration of the fingerprint technique. We studied the core-loss edges from gaudefroyite in the 0 to 1000 eV energy-loss range, and illustrate the uniqueness of the spectra by comparison with those from materials possessing a range of structural and electronic properties. The B *K*-edge from gaudefroyite is consistent with 3-fold-coordinated B and distinct from the edge for 4-fold-coordinated B. The C *K*-edge is distinct from that in elemental C, but consistent with that attributed to the carbonate anion. The Mn $L_{2,3}$-edge exhibits ELNES indicative of octahedrally coordinated Mn^{3+}; it is distinct from the edge shapes for the other Mn oxidation states. The O *K*-edge is rich in structure arising from O in the BO_3^{3-}, CO_3^{2-}, and $Mn^{3+}O_6^{n-}$ groups, with little contribution from the predominantly ionic Ca–O bonds.

Keywords: parallel electron energy-loss spectroscopy, PEELS, electron-loss near-edge structure, ELNES, coordination fingerprint, valence fingerprint, gaudefroyite.

Sommaire

Nous nous sommes servis de la spectroscopie de la perte d'énergie des électrons (PEELS) en parallèle avec un microscope électronique à transmission avec balayage, muni d'un canon d'émission à froid pour obtenir des spectres de haute résolution. Une analyse détaillée de la structure du spectre de perte d'électrons près du seuil d'absorption (ELNES) du noyau donne de l'information à propos de l'état d'oxydation et la symétrie des sites des atomes excités. Dans plusieurs cas, le spectre ELNES

possède une forme qui dépend de la coordinence des atomes voisins et qui fournit donc une "empreinte digitale" de cette coordinence. La gaudefroyite, $Ca_4Mn_3(BO_3)_3(CO_3)(O,OH)_3$, contient plusieurs éléments légers, et sert d'exemple éloquent de la puissance de la technique. Nous avons étudié les seuils de perte d'énergie du noyau de la gaudefroyite dans l'intervalle de 0 à 1000 eV, et nous illustrons la spécificité des spectres en les comparant à ceux de matériaux possédant une gamme de propriétés structurales et électroniques. Le seuil *K* de l'atome B dans la gaudefroyite concorde avec le cas du bore à coordinence 3, et diffère de celui du bore à coordinence 4. Le seuil *K* de l'atome C se distingue de celui du carbone élémentaire, mais il concorde avec celui qui caractérise les groupes anioniques carbonatés. Le seuil $L_{2,3}$ du manganèse possède un spectre ELNES typique du Mn^{3+} en coordinence octaédrique. Ce spectre diffère de ceux des autres valences de Mn. Le seuil *K* de l'oxygène possède une structure riche en détails à cause des contributions de l'oxygène des groupes BO_3^{3-}, CO_3^{2-}, et $Mn^{3+}O_6^{9-}$, mais sans contribution appréciable des liaisons Ca–O, à caractère plutôt ionique.

Mots-clés: spectroscopie en parallèle de la perte d'énergie des électrons, PEELS, structure de la perte d'électrons près d'un seuil, ELNES, "empreinte digitale" de la coordinence, "empreinte digitale" de la valence, gaudefroyite.

INTRODUCTION

Electron energy-loss spectroscopy (EELS) conducted with a transmission electron microscope (TEM) can be used for quantitative chemical analysis at the nanometer scale; it has the added advantage over many common analytical techniques of being able to record information about the light elements. Analysis of the fine structure of EELS spectra offers the possibility of determining important crystal-chemical properties such as the oxidation state, coordination, and site symmetry. As an example of the power of EELS in mineralogy, we present spectra for gaudefroyite, a complex boro-carbonate, and compare them to those for a range of minerals and synthetic materials of known structure.

Gaudefroyite contains 3-fold coordinated B and C, 7- and 9-fold coordinated Ca, and 6-fold coordinated Mn^{3+}. Its idealized formula is $Ca_4Mn_3(BO_3)_3(CO_3)O_3$, although the Mn sites are not fully occupied, but range from $Mn_{2.68}$ to $Mn_{2.81}$. Substitution of OH^- for O compensates for the Mn deficiency (Beukes *et al.* 1993). Gaudefroyite has been the subject of several studies (Jouravsky & Permingeat 1964, Yakubovich *et al.* 1975, Beukes *et al.* 1993, Garvie, Groy and Buseck, in prep.). It occurs in the hydrothermal Mn deposits near Tachgagalt in Morocco (Jouravsky & Permingeat 1964) and in the Kalahari manganese field in South Africa. The Kalahari gaudefroyite is a late secondary phase formed at high temperatures and low pressures during B metasomatism (Beukes *et al.* 1993).

Intensity maxima called core-loss edges are caused by transitions of core electrons to unoccupied states in the conduction band. These edges sit on a monotonically decreasing background; the initial rise in intensity is called the edge threshold. The edges can take a variety of shapes (*e.g.*, Colliex *et al.* 1985, Egerton 1986), but within the first ~30 to 50 eV of the edge threshold, there commonly are a number of pronounced peaks. This near-edge region of a core-loss edge is defined as the electron energy-loss near-edge structure (ELNES). Extending to several hundred eV above the ELNES is a region dominated by the extended electron energy-loss fine structure (EXELFS). Energy-loss features at higher energies, such as the *K*-edges of Ca (~4000 eV) and Mn (~6535 eV), are not amenable to EELS study in a TEM, but can be recorded by X-ray absorption spectroscopy (XAS) (*e.g.*, Manceau *et al.* 1992). Close to the edge threshold, the ELNES represents transitions to unoccupied states modified by the immediate environment of the atom. In many cases, the ELNES exhibits a shape reflecting the nearest-neighbor coordination. Such a shape is referred to as a coordination "fingerprint"; similarly, for certain elements, a fingerprint of the oxidation state is observed. At high-energy resolution, certain elements such as Fe and Ti exhibit edge features indicative of both coordination and oxidation state.

The recent commercial availability of parallel recording systems for EELS (PEELS) conducted in conjunction with a TEM has resulted in an increase in EELS-related studies. The use of PEELS, as opposed to serial EELS, results in a large gain in collection efficiency. ELNES data can now be recorded rapidly and from materials that were too beam-sensitive to be collected with serial EELS at comparable spatial resolutions.

In this study, we demonstrate how interpretation of the ELNES associated with a core-loss edge is used to obtain chemical and structural properties from minerals. We use the ELNES to infer the nearest-neighbor coordination of the atoms undergoing excitation and, where appropriate, their oxidation state.

INTERPRETATION OF ELECTRON-LOSS NEAR-EDGE STRUCTURES

Core-loss edges recorded at low scattering angles obey the dipole selection rules, which state that during electron excitations, the change in angular momentum, l, obeys $\Delta l = \pm 1$, whereas the spin remains unchanged, $\Delta s = 0$. At high scattering angles (large momentum transfers), nondipole transitions can contribute significantly to an EELS spectrum (Auerhammer & Rez 1989). Core-loss *K*-edges are caused by the excitation of core 1s electrons ($l = 0$) to unoccupied states of p-like symmetry ($l = 1$). The core wavefunctions of an

atom in a solid show little difference in energy from an isolated atom. On the other hand, the energies and character of the outer bonding and antibonding orbitals, which form bands of orbitals, are governed by the bonding and oxidation state of the atoms. Thus, since the core-loss edges represent transitions to these unoccupied states, we expect to see modifications to the ELNES that reflect the bonding. Before excitation, the initial state is well defined, but in the final state, a core hole is present. The core hole is expected to modify the final state, but the extent to which this is done depends on, among other factors, the atomic number and character of the atom (Brydson 1991, Tamura *et al.* 1995).

The $L_{2,3}$-edges result from the excitation of 2p core states ($l = 1$) to unoccupied s ($l = 0$) and d ($l = 2$) states. The $L_{2,3}$ ELNES from the 3d transition metals (TM), including K and Ca, consist of two intense peaks arising from dipole-allowed transitions from an initial $2p^63d^n$ state to a final $2p^53d^{n+1}$ state. K^+ and Ca^{2+} have empty d-orbitals in their initial states, so the excitation is of the form $2p^63d^0 \rightarrow 2p^53d^1$. The L_3- and L_2-edges are caused by the two ways in which the spin, *s*, can couple with the orbital angular momentum, *l*, to give the total angular momentum, *j*. The L_3-peak is caused by transitions from the $2p_{3/2}$ level, and the L_2-edge, from the $2p_{1/2}$ level. Transitions to the dipole-allowed s-like states only have a small effect on the $L_{2,3}$-edges and are manifested as weak structures at higher energies above the $L_{2,3}$ peaks (Abbate *et al.* 1992). In the presence of surrounding ligands, the 3d TM $L_{2,3}$ ELNES will be modified by the crystal field from the ligands.

Materials and Methods

We studied a 5-mm crystal of gaudefroyite from the Kalahari locality. It is dark brown with a stubby habit and hexagonal shape; its identity was confirmed by powder X-ray diffraction. Microprobe and secondary-ion mass spectroscopy analysis failed to show signs of zoning or inclusions. The sample was prepared for PEELS analysis by crushing a mm-sized piece in acetone and drying a drop of the finely ground mineral in suspension on a lacy C film supported on a copper TEM grid.

The remaining samples (Table 1) used in this study come from a variety of sources as either well-characterized single crystals or pure inorganic solids. The metallic Mn, Ca, and CaO were prepared *in situ* in the electron microscope by electron-beam reduction of calcite or metallic Mn containing a few wt% of O. After electron-beam irradiation of a ~3-μm piece of Mn, fingers of thin electron-beam-transparent Mn grew from the sides of the larger particle, free of the O present in the parent material. The rest of the samples studied, except for TiC, β-rhombohedral boron (β-B_{105}), and glassy B_2O_3, are minerals.

Spectra were acquired with a Gatan 666 PEELS spectrometer attached to the top of a VG HB5 scanning transmission electron microscope (STEM). The HB5 was equipped with a cold field-emission gun (FEG) and operated at 100 kV with an emission current of 5 μA, a probe semiangle of ~11 mrad, and a collection angle of 12.5 mrad. Under these conditions, the resolution of the STEM PEELS system was ~0.4 eV. The spectrometer was calibrated against the Ni L_3-edge from NiO, which was determined to be at 853.2 eV by XAS (van der Laan *et al.* 1986).

To reduce C contamination in the STEM, the TEM grid supporting the finely crushed material was placed on a 100 Watt light bulb for ~10 minutes just prior to insertion in the STEM. A thermocouple placed on the bulb gave a reading of ~170°C. Failure to place the sample on the bulb invariably resulted in the buildup of carbonaceous material during the recording of PEELS data, which was a problem since the C *K*-edge from the contamination interfered with the

TABLE 1. MINERALS AND SYNTHETIC COMPOUNDS STUDIED BY PEELS

	Ideal formula	Localities/Source
asbolane	$(Co,Ni)_{1-y}(MnO_2)_{2-x}(OH)_{2-2y+2x}.nH_2O$	Gebe Island, Indonesia
calcite	$CaCO_3$	Llanelwedd Quarry, Wales
datolite	$CaBSiO_4OH$	Kalahari manganese field, South Africa
diamond	C	Southern Africa
fluorite	CaF_2	unknown
gaudefroyite	$Ca_4Mn_{3-x}(BO_3)_3(CO_3)(O,OH)_3$	Kalahari manganese field, South Africa
graphite	C	South Western Graphite Mine, Texas
ludwigite	$Mg_2Fe^{3+}BO_5$	Skye, Scotland
manganite	γ-MnOOH	Black Jack Mine, Arizona
piemontite	$Ca_2MnAl_2O(SiO_4)(Si_2O_7)(OH))$	St. Marcel, Piemont, Italy
rhodochrosite	$MnCO_3$	unknown
rhodizite	$(Cs,K)Be_4Al_4(B,Be)_{12}O_{28}$	Antsirabe, Madagascar
metallic calcium	Ca	prepared *in situ**
metallic manganese	Mn	prepared *in situ**
calcium oxide	CaO	prepared *in situ**
titanium carbide	$TiC_{0.98}$	commercial
β-rhombohedral boron	β-B_{105}	commercial
glassy boric oxide	B_2O_3	commercial

* see text for preparation details.

C *K*-edge from the material under investigation.

Core-loss edges were obtained from thin areas, typically ~50 nm thick, overhanging holes in the lacy C film. The B and C *K*-edges were recorded with integration times of ~1 s. The remaining edges were recorded with integration times of 4 to 8 s. Spectra were acquired by scanning a focused probe, diameter 1 nm, in a TV-rate raster over regions measuring 15×10 nm^2. In principle, the spatial resolution in the HB5 STEM is governed by the size of the probe, which is typically 1 nm in diameter; probe sizes down to 2.2 Å have been used to probe individual atomic columns (Browning *et al.* 1993). In practice, the spatial resolution is dictated by the resistance of the materials being studied to electron-beam damage. An energy dispersion of 0.1 eV was used, allowing the fine structure of the edges to be recorded. The dark current and a background of the form AR^{-r} (Egerton 1986) were subtracted from beneath each core-loss edge, and the effect of the asymmetry of the zero-loss peak was deconvoluted following the procedures of Egerton.

Electron Loss Near-Edge Structures

The core-loss edges from gaudefroyite are shown in Figure 1, and the principal energies listed in Table 2. Subsequent figures compare the individual core-loss edges from gaudefroyite with edges from compounds that are used to explain the gaudefroyite ELNES. The individual edges are described in order of increasing energy losses, B and C *K*-edges, Ca $L_{2,3}$-edge, O *K*-edge, and the Mn $L_{2,3}$-edge.

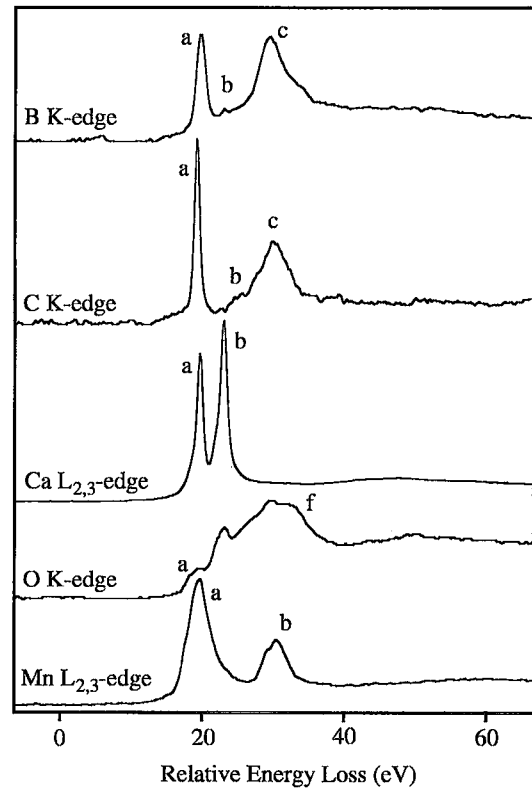

FIG. 1. Core-loss edges from gaudefroyite. The letters refer to prominent features described in the text and Table 2. The spectra have been aligned relative to the first peak a.

Boron

In minerals, B, which is bonded almost exclusively to O or OH^-, occurs in the tetrahedral BO_4^{5-}, and the planar triangular BO_3^{3-} groups. The O atoms may be partially or totally replaced by OH^-. The spectra from gaudefroyite, ludwigite, and glassy B_2O_3 exhibit similar ELNES, dominated by a prominent peak at ~193.6 eV and a broader asymmetrical peak centered around 204 eV (Fig. 2). Boron in rhodizite is tetrahedrally coordinated, and its B *K*-edge differs from the $^{[3]}$B *K* ELNES. The differences between the $^{[3]}$B and $^{[4]}$B *K* ELNES can be used to determine the $^{[3]}$B/$^{[4]}$B ratio in minerals containing B in both coordinations (Sauer *et al.* 1993, Garvie 1995, Garvie *et al.* 1995). Both ludwigite and glassy B_2O_3 contain $^{[3]}$B, and their B *K*-edges are similar to that of gaudefroyite. The good match between these materials allows us to conclude that the B in gaudefroyite is 3-fold-coordinated.

An understanding of core-loss edge features can be undertaken using a number of theoretical techniques (Brydson 1991, de Groot 1993, Rez *et al.* 1995). Of these, the molecular orbital (MO) methods are intuitively the easiest to understand because particular features of the ELNES are assigned to transitions to specific MOs. In turn, these MOs are governed by the bonding between the central atom in the polyatomic cluster and the surrounding ligands. Since the B *K*-edge reflects transitions to unoccupied p-like states, these edges presumably reflect the p-like unoccupied density of states. A MO model for BO_3^{3-} indicates that the

TABLE 2. ABSOLUTE ENERGIES (eV) OF THE PRINCIPAL FEATURES OF THE CORE-LOSS EDGES FROM GAUDEFROYITE

	element				
peaks	B	C	Ca	O	Mn
a''	–	–	347.0	–	639.9
a'	–	–	347.8	–	641.4
a	193.6	290.1	349.1	530.3	642.4
b'	–	–	351.0	–	651.7
b	196.8	295.1	352.5	531.4	653.1
c'	–	–	–	534	–
c	203.1	300.7	–	535.1	–
d	–	–	–	538.9	–
e	–	–	–	541.6	–
f	–	–	–	544.0	–

Note: error in EELS values is ±0.2 eV

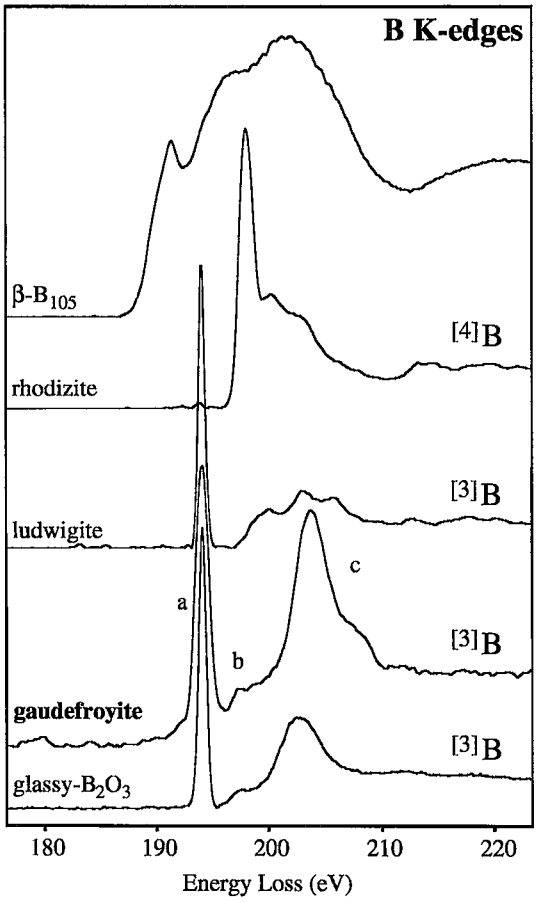

FIG. 2. B *K*-edges from gaudefroyite, β-rhombohedral boron (β-B_{105}), rhodizite [$^{[4]}$B; $(K,Cs)Be_4Al_4(B,Be)_{12}O_{28}$], ludwigite ($^{[3]}$B; Mg_2FeBO_5) and glassy B_2O_3 ($^{[3]}$B). The coordination of the B in the minerals is shown to the right of the spectra. The spectra illustrated here and in subsequent figures are shown on an arbitrary scale of intensity.

lowest unoccupied MOs are the a''_2 (π*), a'_1 (σ*), and e′ (σ*) orbitals derived from B2p, B2s, and B2p electrons, respectively (Vaughan & Tossell 1973, Tossell 1986). On the basis of the MO scheme, peaks a and c for the $^{[3]}$B *K*-edge from gaudefroyite are assigned to states of a''_2 (π*) and e′ (σ*) character, respectively. The origin of peak b is likely caused by the interaction of non-nearest neighbors, *i.e.*, interactions between B and atoms beyond the BO_3^{3-} anion (Garvie *et al.* 1994).

The B *K*-edges of $^{[3]}$B and $^{[4]}$B exhibit distinct ELNES arising from the different MO structures of BO_3^{3-} and BO_4^{5-}. The rhodizite B *K*-edge consists of an initial sharp rise in intensity, with a maximum at 198.0 eV, followed by weaker fluctuations at 200.2, 203.1, and 213.3 eV. The MO model for the BO_4 group shows the first unoccupied MO to be the triply degenerate t_2 (σ*) followed by the a_1 MO (Vaughan & Tossell 1973). The strong peak at 198.0 eV is assigned to transitions to the t_2 (σ*) MO. The origin of the features immediately following the main peak are uncertain, but they are possibly caused by higher unoccupied MOs from the BO_4^{5-} anion and interactions with the surrounding atoms.

Finally, the spectrum for β-B_{105} (the subscript refers to the number of B atoms in the unit cell) differs significantly from the B *K*-edges of $^{[3]}$B or $^{[4]}$B. The lower energy of the edge onset relative to the B *K*-edges from $^{[3]}$B and $^{[4]}$B is caused by the lower effective positive charge on the B in β-B_{105}. In general, edge onsets shift to higher energies as the formal oxidation state of the excited atoms increases, an effect known as the chemical shift.

Carbon

The C *K*-edge from gaudefroyite exhibits similar ELNES to the $^{[3]}$B *K*-edge (Fig. 3), which is a consequence of the isoelectronic and isostructural nature of

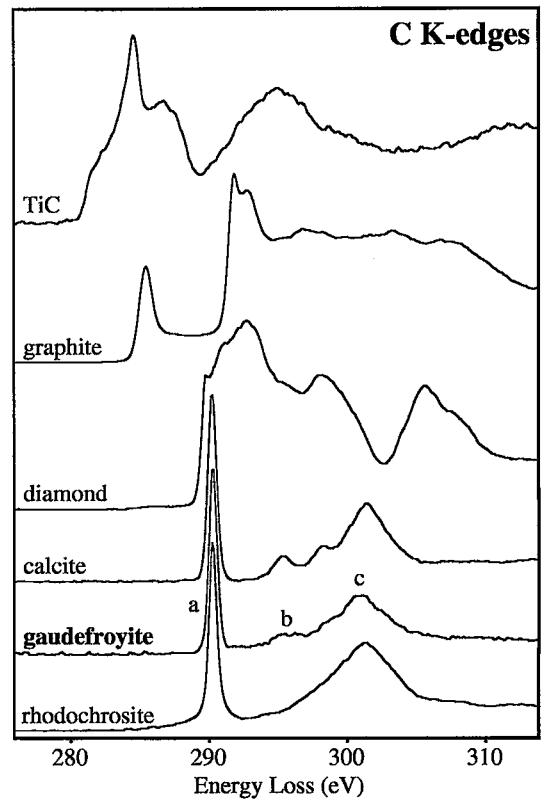

FIG. 3. C *K*-edge from gaudefroyite, cubic TiC, graphite, diamond, calcite ($CaCO_3$), and rhodochrosite ($MnCO_3$).

the trigonal CO_3^{2-} and BO_3^{3-} anions. A similar edge shape is also present for the N *K*-edge from the NO_3^- anion (Nekipelov *et al.* 1988). By analogy with the B *K* ELNES, the principal features of the C *K*-edge from gaudefroyite arise from transitions to unoccupied states of π* (peak a) and σ* (peak c) character, respectively. The C *K*-edges from rhodochrosite and calcite are illustrated in Figure 3. The C *K*-edges from the three minerals are similar, thus providing the basis for a fingerprint of the coordination.

Spectra of a selection of other carbon species (Fig. 3) are markedly different, illustrating the sensitivity of the ELNES to the nearest-neighbor environment. Such differences have been used to identify the nature of the C in interplanetary dust particles (Keller *et al.* 1994), to determine the ratio of amorphous and graphitic C in carbonaceous aerosols (Katrinak *et al.* 1992), and to understand the bonding in transition metal carbides (Craven & Garvie 1995).

The increasing energy-losses of the C *K*-edge on going from TiC (280.4 eV) to graphite (284.2 eV) and the carbonate anion (288.5 eV) can be understood in relation to the changing charges on the C atom. In TiC, graphite, and CO_3^{2-}, the C atoms are essentially negative, neutral, and positive, respectively. The chemical shift cannot be understood solely from the valence of the excited atom, as can be demonstrated by comparing the C *K*-edges from graphite, which is an electrical conductor, and diamond, which is an insulator with a band gap of 5.5 eV. In comparison to graphite, the C *K*-edge onset from diamond has shifted to higher energy losses, reflecting this band gap, and thus in this case the chemical shift is related to differences in bonding and not to changes in the valence of the excited atom.

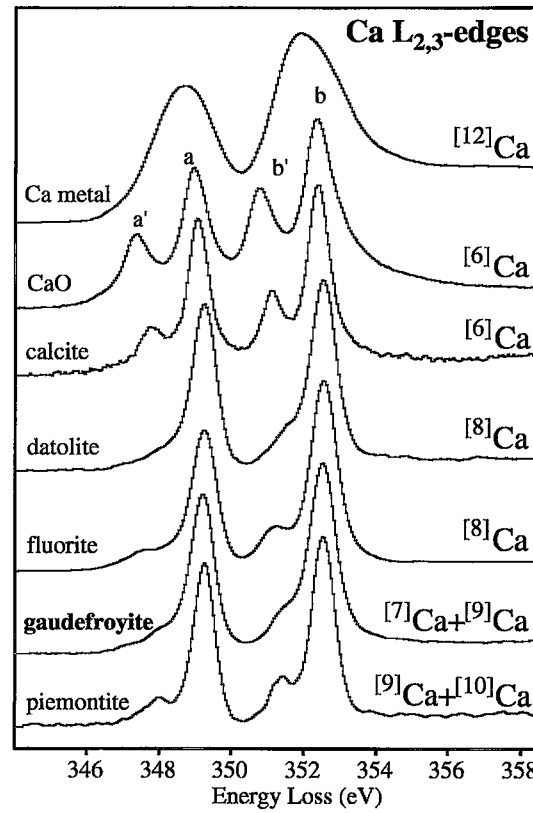

FIG. 4. The Ca $L_{2,3}$-edge from gaudefroyite ([7]Ca and [9]Ca), elemental Ca ([12]Ca), CaO ([6]Ca), calcite ([6]Ca; $CaCO_3$), datolite [[8]Ca; $CaBiSiO_4(OH)$], fluorite ([8]Ca; CaF_2), and piemontite [[9]Ca and [10]Ca; $Ca_2MnAl_2O(SiO_3)(Si_2O_7)(OH)$]. The coordination of the Ca is shown to the right of the spectra.

Calcium

Since Ca in minerals is found exclusively in the 2+ oxidation state, differences among the Ca $L_{2,3}$ ELNES from different minerals should reflect the local environment surrounding the Ca atoms. We wanted to confirm the coordination number and site symmetry of the Ca polyhedra in gaudefroyite and determine the ratios of the coordinations from the Ca $L_{2,3}$ ELNES. The Ca $L_{2,3}$-edges from several Ca-bearing materials consist of two intense peaks, a and b (Fig. 4), with only small variations in the energy of the L_3-peak maxima.

Since the Ca environment in gaudefroyite is complex, with distorted 7- and 9-fold coordinated polyhedra, we first discuss the spectrum obtained from CaO, in which the Ca atoms sit in a regular octahedral environment, with six identical Ca – O bond lengths of 2.405 Å. The Ca 3d orbitals are split into a lower-energy t_{2g} level and a higher-energy e_g level. The Ca $L_{2,3}$ spectrum consists of two principal peaks, a and b, separated by 3.4 eV, and two weaker peaks, a′ and b′, separated by 1.61 eV from the following peak. In calcite, Ca is octahedrally coordinated, and its Ca $L_{2,3}$-edge is similar to that from CaO. Thus, for octahedrally coordinated Ca with O_h site symmetry, as in CaO and calcite, the Ca $L_{2,3}$-edges seem to exhibit coordination-specific ELNES.

Interpretation of the gaudefroyite Ca $L_{2,3}$ ELNES as well as that from datolite and piemontite is complex because of the two types of polyhedra in gaudefroyite and piemontite and the 8-fold coordinated polyhedra in datolite and fluorite. Himpsel *et al.* (1991) have shown that the Ca $L_{2,3}$-edge from fluorite is not easy to interpret with the simple crystal-field model. By comparing the gaudefroyite Ca $L_{2,3}$-edge with that from CaO and calcite, we can deduce that Ca in gaudefroyite is unlikely to be located in a regular octahedral environment because of the differences among the spectra. A thorough understanding of the ELNES, in relation to the Ca environment, requires modeling of the edges,

such as has been done by Himpsel *et al.* (1991) for fluorite.

Oxygen

Whereas with B and C, we can explain the corresponding *K*-edges as caused by single coordinated sites, O occurs in several coordinations and is bonded to a variety of different atoms. In general, if a compound containing a "molecular unit", such as CO_3^{2-}, in which the bonding is predominantly covalent, is ionically bonded to a cation such as Ca, then the edge shapes from the two atoms within the "molecular unit" will exhibit basically the same ELNES; there will be little contribution to the O *K*-edge from the ionically bonded cation. Thus we expect the principal features on the gaudefroyite O *K*-edge to arise from O in the BO_3^{3-}, CO_3^{2-}, and $Mn^{3+}O_6^{n-}$ groups, where the cation – O bonding is predominantly covalent, with little contribution from the mainly ionic Ca – O bonds.

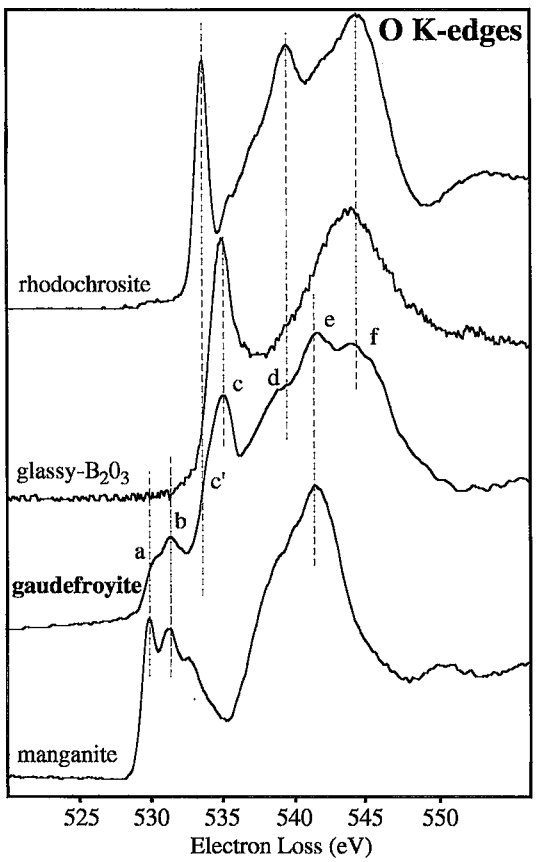

FIG. 5. O *K*-edges from rhodochrosite (O associated with CO_3^{2-}; $MnCO_3$), glassy B_2O_3 (O bonded to the BO_3^{3-}) and manganite (O associated with the MnO_6 octahedron; γ-MnOOH). The absolute energies of the labeled features are compared in Table 3.

TABLE 3. ABSOLUTE ENERGIES (eV) OF THE PRINCIPAL FEATURES OF THE SPECTRA IN FIGURE 5

	peaks						
Minerals	a	b	c'	c	d	e	f
gaudefroyite	530.3	531.4	534	535.1	538.9	541.6	544
rhodochrosite	–	–	534.0	–	539.9	–	544.7
glassy B_2O_3	–	–	–	535.0	–	–	544.0
manganite	530.0	531.4	–	–	–	541.5	–

Note: error in EELS values is ±0.2 eV

In order to assign the features on the O *K*-edge as arising from particular cation – O bonds, we compare the absolute energies of the principal features for the O *K*-edges from rhodochrosite, glassy B_2O_3, and manganite with the O *K*-edge from gaudefroyite (Fig. 5, Table 3). All the main features in the oxide spectra also occur in the gaudefroyite O *K*-edge.

Manganese

In nature, Mn occurs as Mn^{2+}, Mn^{3+}, and Mn^{4+}. Figure 6 illustrates the Mn $L_{2,3}$-edges from asbolane (Mn^{4+}), gaudefroyite (Mn^{3+}), manganite (Mn^{3+}), rhodochrosite (Mn^{2+}), and Mn metal. With increase in oxidation state, the Mn $L_{2,3}$-edges for the non-metal show three apparent changes: a valence-specific edge shape, a decrease in the L_3/L_2 area ratio, and a move to higher energy-losses of the L_3- and L_2-edges (Rask *et al.* 1987, Garvie & Craven 1994a, b). Table 4 summarizes the relevant data for the Mn $L_{2,3}$-edges.

Manganite and gaudefroyite have almost identical Mn $L_{2,3}$ ELNES, a result of the similar coordination and oxidation state of Mn in both minerals. The L_3 peak maximum for gaudefroytite at 642.4 eV, peak a, lies between the values for the L_3 peak maxima for the Mn^{2+} and Mn^{4+} compounds. The four 3d electrons in the Mn^{3+} compounds cause the MnO_6 octahedron to distort, with elongation of the two *trans* bonds but little difference in the four equatorial Mn–O distances. This Jahn–Teller distortion reduces the symmetry of the octahedron from O_h to D_{4h}. For weak-field tetragonal distortions, as found for the MnO_6 octahedra in manganite and gaudefroyite, the t_{2g} and e_g MOs are further split into four orbitals (Lever 1984). The L_3-edge from gaudefroyite exhibits two partially resolved peaks, a′ and a″, that are 1 eV and 2.4 eV below the peak maximum, respectively. The partially resolved structures on the Mn L_3 ELNES from manganite and gaudefroyite represent transitions to unoccupied states based on a crystal-field splitting of the 3d states in weak-field D_{4h} site symmetry (Garvie & Craven 1993, 1994b).

Rhodochrosite has an Mn $L_{2,3}$-edge characterized by a strong L_3 peak and a weaker L_2 peak. The L_3-edge exhibits several resolvable peaks, with a maximum

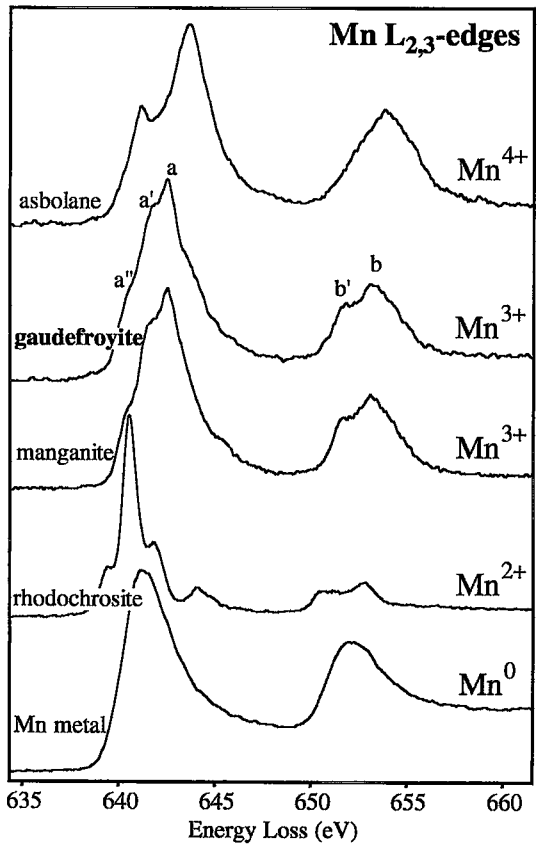

FIG. 6. The Mn $L_{2,3}$-edges from gaudefroyite, metallic Mn, asbolane (Mn^{4+}), manganite (Mn^{3+}), and rhodochrosite (Mn^{2+}). The oxidation state of the Mn is shown to the right of the spectra.

at 640.3 eV and a small pre-peak 1.12 eV lower in energy. Their energy separation has been interpreted as a measure of the crystal-field strength acting on the Mn (Garvie & Craven 1994b).

The asbolane ($^{[6]}Mn^{4+}$) Mn L_3-edge exhibits two peaks, a maximum at 643.8 eV and a weaker peak at 641.4 eV. For the L_3-edges from Mn^{4+} materials, the lower-energy peak arises from transitions to unoccupied states with t_{2g} MO character, and the more intense peak, from transitions to unoccupied states of e_g MO character. The dominantly covalent Mn–O bonding in Mn^{4+} minerals explains the MO-like nature of this edge (Garvie & Craven 1994b), as opposed to the quasiatomic model that adequately describes many 3d transition metal (TM) $L_{2,3}$-edges (de Groot *et al.* 1989, 1990a, b, van der Laan & Kirkman 1992).

TABLE 4. ABSOLUTE ENERGIES OF THE L_3-EDGE AND THE L_3/L_2 AREA RATIOS FOR SELECTED Mn-BEARING COMPOUNDS

Material	L_3-edge	L_3/L_2 area ratio
rhodochrosite	640.4	4.67
manganite	642.5	2.55
gaudefroyite	642.4	2.46
asbolane	643.8	2.17

The Mn $L_{2,3}$-edge from Mn metal exhibits two broad peaks centered at 641.3 and 652.0 eV. The lack of ELNES is a result of the screening of the core hole by the valence electrons.

DISCUSSION

We have shown the ease with which the coordination of light elements can be determined from crystals having nanometer dimensions. The B *K*-edge from gaudefroyite is clearly attributed to $^{[3]}B$ rather than $^{[4]}B$. As expected, the gaudefroyite C *K*-edge is consistent with that from the C *K*-edge of the carbonate anion. The C and B *K* ELNES are indicative of the 3-fold environment and can be interpreted in the light of a MO model for the CO_3^{2-} and BO_3^{3-} anions.

Few investigations have concentrated on the near-edge structure of the Ca $L_{2,3}$-edges, and these have largely been confined to XAS studies (Himpsel *et al.* 1991, Borg *et al.* 1992). The lack of prior Ca $L_{2,3}$ ELNES studies results from the high-energy resolution required to resolve the ELNES. The Ca $L_{2,3}$-edge from gaudefroyite does not show any edge features that could be attributed to the two coordinations of the Ca, but we were able to show that the Ca in gaudefroyite is not dominantly octahedrally coordinated. Octahedrally coordinated Ca exhibits clearly resolved ELNES that may reflect the strength of the crystal field, although the overall $L_{2,3}$ structure is similar for all the Ca compounds.

The gaudefroyite O *K*-edge exhibits ELNES rich in structure because of the many different O environments. We assign these structures to the covalent cation – O bonding within the structure. The O *K*-edge peaks at *ca.* 530 eV are indicative of covalent bonding between at least some of the O atoms and 3d TM.

For the Mn $L_{2,3}$-edge, the shape and energy position of the L_3 peak indicate the oxidation state. The valence-specific edge shapes can be used as the basis for determining the ratio of oxidation states in mixed valence 3d TM compounds. Such a determination has been demonstrated by Cressey *et al.* (1993) for Fe-bearing minerals having mixed valency and coordination, and Pattrick *et al.* (1993) for Cu-bearing minerals. Comparison of the Mn $L_{2,3}$-edge from gaudefroyite with the spectra in Figure 6 demonstrates that the Mn is in the 3+ oxidation state. Interpretation of the first series $L_{2,3}$-edges can be achieved *via* a quasiatomic model with the inclusion of solid-state effects, most notably the crystal field.

Conclusions

PEELS conducted in a TEM is a powerful spectroscopic technique providing important information on chemical composition and bonding. The possibility of using the ELNES as a probe of the local electronic structure was demonstrated by studying gaudefroyite. Analysis of the core-loss edges illustrates the ease with which element identification can be undertaken, even for elements such as B, C, and O, which are traditionally difficult to deal with by energy-dispersion spectroscopy, although recent advances in electron-probe micro-analysis hold promise for materials containing the light elements of Z from 4 to 9 (Raudsepp 1995, Hawthorne *et al.* 1995). Analysis of the core-loss fine structure, and comparison of the edge shapes with materials in which the bonding of the elements is known, allowed the coordination of B and C and the oxidation state of Mn in gaudefroyite to be determined.

Acknowledgements

We thank Dr. J. Faithfull of the Hunterian Museum, Glasgow, for providing samples of rhodochrosite (Rotley 1425) and piemontite (M8006). In addition, we thank Drs. A. Manceau and R.F. Martin for comments and suggestions. PEELS data were recorded in the Department of Physics and Astronomy at the University of Glasgow. LAJG and AJC thank the Engineering and Physical Sciences Research Council for providing funds to purchase the Gatan 666 parallel electron loss spectrometer. Partial funding was provided by National Science Foundation grant EAR 921 9376 (to PRB).

References

Abbate, M., de Groot, F.M.F., Fuggle, J.C., Fujimori, A., Strebel, O., Lopez, F., Domke, M., Kaindl, G., Sawatzky, G.A., Takano, M., Takeda, Y., Eisaki, H. & Uchida, S. (1992): Controlled-valence properties of $La_{1-x}Sr_xFeO_3$ and $La_{1-x}Sr_xMnO_3$ studied by soft-x-ray absorption spectroscopy. *Phys. Rev.* **B 46**, 4511-4519.

Auerhammer, J.M. & Rez, P. (1989): Dipole-forbidden excitations in electron-energy-loss spectroscopy. *Phys. Rev.* **B 40**, 2024-2030.

Beukes, G.J., de Bruiyn, H. & van der Westhuizen, W.A. (1993): Gaudefroyite from the Kalahari manganese field, South Africa. *Neues Jahrb. Mineral., Monatsh.*, 385-392.

Borg, A., King, P.L., Pianetta, P., Lindau, I., Mitzi, D.B., Kapitulnik, A., Soldatov, A.V., Della Longa, S. & Bianconi, A. (1992): Ca 3d unoccupied states in $Bi_2Sr_2CaCu_2O_8$ investigated by Ca $L_{2,3}$ x-ray-absorption near-edge structure. *Phys. Rev.* **B 46**, 8487-8495.

Browning, N.D., Chisholm, M.F. & Pennycook, S.J. (1993): Atomic-resolution chemical analysis using a scanning transmission electron microscope. *Nature* **366**, 143-146.

Brydson, R. (1991): Interpretation of near-edge structure in the electron energy-loss spectrum. *Bull. Elect. Microscopy Soc. Am.* **21**, 57-67.

Colliex, C., Manoubi, T., Gasgnier, M. & Brown, L.M. (1985): Near edge fine structures on electron energy loss spectroscopy core-loss edges. *Scanning Electron Microscopy* **II**, 489-512.

Craven, A.J. & Garvie, L.A.J. (1995): Electron energy loss near edge structure (ELNES) on the carbon K-edge in transition metal carbides with the rock salt structure. *Microsc. Microanal. Microstruct.* **6**, 89-98.

Cressey, G., Henderson, C.M.B. & van der Laan, G. (1993): Use of L-edge x-ray absorption spectroscopy to characterize multiple valence states of 3d transition metals; a new probe for mineralogical and geochemical research. *Phys. Chem. Minerals* **20**, 111-119.

Egerton, R.F. (1986): *Electron Energy-Loss Spectroscopy in the Electron Microscope.* Plenum Press, New York, N.Y.

Garvie, L.A.J. (1995): Parallel electron energy-loss spectroscopy of boron in minerals. *Rev. Mineral.* **33** (in press).

_____ & Craven, A.J. (1993): Determination of the crystal-field strength in manganese compounds by parallel electron energy loss spectroscopy. *In* Proc. Electron Microscopy and Analysis Group Conf. **138** (A.J. Craven, ed.). Inst. Physics Publishing Ltd. (31-34).

_____ & _____ (1994a): Electron-beam-induced reduction of Mn^{4+} in manganese oxides as revealed by parallel EELS. *Ultramicroscopy* **54**, 83-92.

_____ & _____ (1994b): High-resolution parallel electron energy-loss spectroscopy of Mn $L_{2,3}$-edges in inorganic manganese compounds. *Phys. Chem. Minerals* **21**, 191-206.

_____, _____ & Brydson, R. (1994): Use of electron-energy loss near-edge fine structure in the study of minerals. *Am. Mineral.* **79**, 411-425.

_____, _____ & _____ (1995): A parallel electron energy-loss spectroscopy (PEELS) study of boron in minerals: the electron energy-loss near-edge structure (ELNES) of the B K-edge. *Am. Mineral.* **80** (in press).

de Groot, F.M.F. (1993): X-ray absorption of transiton metal oxides: an overview of the threoretical approaches. *J. Electron Spectroscopy and Related Phenomena* **62**, 111-130.

_____, Fuggle, J.C., Thole, B.T. & Sawatzky, G.A. (1990a): $L_{2,3}$ x-ray absorption edges of d^0 compounds: K^+, Ca^{2+}, Sc^{3+}, and Ti^{4+} in O_h (octahedral) symmetry. *Phys. Rev.* **B 41**, 928-937.

_____, _____, _____ & _____ (1990b): 2p x-ray absorption of 3d transition-metal compounds: an atomic multiplet description including the crystal-field. *Phys. Rev.* **B 42**, 5459-5468.

———, GRIONI, M., FUGGLE, J.C., GHIJSEN, J., SAWATZKY, G.A. & PETERSEN, H. (1989): Oxygen 1s x-ray-absorption edges of transition-metal oxides. *Phys. Rev.* **B 40**, 5715-5723.

HAWTHORNE, F.C., COOPER, M., BOTTAZZI, P., OTTOLINI, L., ERCIT, T.S. & GREW, E.S. (1995): Micro-analysis of minerals for boron by SREF, SIMS and EMPA: a comparative study. *Can. Mineral.* **33**, 389-397.

HIMPSEL, F.J., KARLSSON, U.O., MCLEAN, A.B., TERMINELLO, L.J., DE GROOT, F.M.F., ABBATE, M., FUGGLE, J.C., YARMOFF, J.A., THOLE, B.T. & SAWATZKY, G.A. (1991): Fine structure of the Ca 2p x-ray-absorption edge for bulk compounds, surfaces, and interfaces. *Phys. Rev.* **B 43**, 6899-6907.

JOURAVSKY, G. & PERMINGÉAT, F. (1964): La gaudefroyite, une nouvelle espèce minérale. *Bull. Soc. franç. Mineral. Cristallogr.* **87**, 216-229.

KATRINAK, K.A., REZ, P. & BUSECK, P.R. (1992): Structural variations in individual carbonaceous particles from an urban aerosol. *Environmental Sci. Technol.* **26**, 1967-1976.

KELLER, L.P., BRADLEY, J.P., THOMAS, K.L. & MCKAY, D.S. (1994): Electron energy-loss spectroscopy of carbon in interplanetary dust particles. *Lunar Planet. Sci.* **25**, 687-688 (abstr.).

VAN DER LAAN, G. & KIRKMAN, I.W. (1992): The 2p absorption spectra of 3d transition metal compounds in tetrahedral and octahedral symmetry. *J. Phys. Cond. Matter* **4**, 4189-4204.

———, ZAANEN, J., SAWATZKY, G.A., KARNATAK, R. & ESTEVA, J.-M. (1986): Comparison of x-ray absorption with x-ray photoemission of nickel dihalides and NiO. *Phys. Rev.* **B 33**, 4253-4263.

LEVER, A.B.P. (1984): *Inorganic Electronic Spectroscopy* (2nd ed.). Elsevier, Amsterdam, Holland.

MANCEAU, A., GORSHKOV, A.I. & DRITS, V.A. (1992): Structural chemistry of Mn, Fe, Co and Ni in manganese hydrous oxides. I. Information from XANES spectroscopy. *Am. Mineral.* **77**, 1133-1143.

NEKIPELOV, S.V., AKIMOV, V.N. & VINOGRADOV, A.S. (1988): X-ray K absorption near-edge fine structure of planar nitrogen-containing oxyanions in crystals. *Sov. Phys. Solid State* **30**, 2095-2097.

PATTRICK, R.A.D., VAN DER LAAN, G., VAUGHAN, D.J. & HENDERSON, C.M.B. (1993): Oxidation state and electronic configuration determination of copper in tetrahedrite group minerals by L-edge x-ray absorption spectroscopy. *Phys. Chem. Minerals* **20**, 395-401.

RASK, J.H., MINER, B.A. & BUSECK, P.R. (1987): Determination of manganese oxidation states in solids by electron energy-loss spectroscopy. *Ultramicroscopy* **21**, 321-326.

RAUDSEPP, M. (1995): Recent advances in the electron-probe micro-analysis of minerals for the light elements. *Can. Mineral.* **33**, 203-218.

REZ, P., BRULEY, J., BROHAN, P., PAYNE, M. & GARVIE, L.A.J. (1995): Calculation of near edge structure. *Ultramicroscopy* **59**, 159-167.

SAUER, H., BRYDSON, R., ROWLEY, P.N., ENGEL, W. & THOMAS, J.M. (1993): Determination of coordinations and coodination-specific site occupancies by electron energy-loss spectroscopy: an investigation of boron-oxygen compounds. *Ultramicroscopy* **49**, 198-209.

TAMURA, E., VAN EK, J., FRÖBA, M. & WONG, J. (1995): X-ray absorption near edge structure in metals: relativistic effects and core-hole screening. *Phys. Rev. Lett.* **74**, 4889-4902.

TOSSELL, J.A. (1986): Studies of unoccupied molucular orbitals of the B–O bond by molecular orbital calculations, X-ray absorption near edge, electron transmission, and NMR spectroscopy. *Am. Mineral.* **58**, 765-770.

VAUGHAN, D.J. & TOSSELL, J.A. (1973): Molecular orbital calculations on beryllium and boron oxyanions: interpretation of X-ray emission, ESCA, and NQR spectra and of the geochemistry of beryllium and boron. *Am. Mineral.* **58**, 765-770.

YAKUBOVICH, O.V., SIMONOV, M.A. & BELOV, N.V. (1975): Structure refinement for gaudefroyite. *Sov. Phys. Crystallogr.* **20**, 87-88.

Received February 15, 1995, revised manuscript accepted August 6, 1995.